Smart Structures and Systems, *Vol. 30, No. 1* (*2022*) *49-62*
https://doi.org/10.12989/sss.2022.30.1.049

Study of compressive behavior of triple joints using experimental test and numerical simulation

Vahab Sarfarazi*[1], Xiao Wang [2], Mojtaba Nesari [3] and Erfan Zarrin Ghalam [3]

[1] *Department of Mining Engineering, Hamedan University of Technology, Hamedan, Iran*
[2] *School of Civil Engineering, Southeast University, Nanjing, China*
[3] *Department of Mining Engineering, Hamedan University of Technology, Hamedan, Iran*

(*Received March 1, 2021, Revised November 3, 2021, Accepted April 3, 2022*)

Abstract. Experimental and discrete element methods were used to investigate the effects of triple joints lengths and triple joint angle on the failure behavior of rock mass under uniaxial compressive test. Concrete samples with dimension of 20 cm × 20 cm × 5 cm were prepared. Within the specimen, three imbedded joint were provided. The joint lengths were 2 cm, 4cm and 6 cm. In constant joint lengths, the angle between middle joint and other joints were 30°, 60°, 90°, 120° and 150°. Totally 15 different models were tested under compression test. The axial load rate on the model was 0.05 mm/min. Concurrent with experimental tests, the models containing triple joints, length and joint angle are similar to the experiments, were numerical by Particle flow code in two dimensions (PFC2D). Loading rate in numerical modelling was 0.05 mm/min. Tensile strength of material was 1 MPa. The results show that the failure behaviors of rock samples containing triple joints were governed by both of the angle and the length of the triple joints. The uniaxial compressive strengths (UCS) of the specimens were related to the fracture pattern and failure mechanism of the discontinuities. Furthermore, it was shown that the compressive behavior of discontinuities is related to the number of the induced tensile cracks which are increased by decreasing the joint length. Along with the damage failure of the samples, the acoustic emission (AE) activities are excited. There were only a few AE hits in the initial stage of loading, then AE hits rapidly grow before the applied stress reached its peak. In addition, every stress drop was accompanied by a large number of AE hits. Finally, the failure pattern and failure strength are similar in both methods i.e., the experimental testing and the numerical simulation methods.

Keywords: acoustic emission; failure behaviors; particle flow code; physical test; triple-joint

1. Introduction

Rock mass is a geological structure that is characterized by many joints. Under the interference of external forces, cracks in rock mass will open or run through, and the merging behavior of cracks has an important effect on the stability of rock engineering, e.g., Underground cavern and slope. It is of great engineering value to study the mechanical behavior of fractured rock mass. From 1960s, by studying the distribution of primary cracks in rock mass, some scholars have revealed the influence of cracks on the properties of fractured rock mass. Brace and Bombolakis (1963) studied the growth of cracks in photoelastic material and glass under compression as part of an investigation of brittle fracture of rock. Price (1966), for the first time, combined the theoretical study with the experiment, investigated the fracture phenomena of brittle and semi brittle rocks during tectonic movement. Based on Griffith's microcrack theory, combined with theoretical analysis and experimental research, Lajtai (1971) analyzed the restraining effect of confining pressure on tensile crack and the deterioration effect of shear crack propagation on material; Shen *et al*. (2004) studied the crack propagation law of sandstone under uniaxial compression with different stress levels and loading rates at the micro scale, and pointed out that the asymmetry of crack propagation and the surface crack are the reflection of internal crack propagation. Ashby and Hallam (1986) investigated the fracture characteristics of brittle materials, and considered that the crack initiation stress is related to the geometric characteristics, friction coefficient and stress state of the crack, and the crack propagation and penetration is the fundamental reason for the unstable propagation and instability of materials. After the 1990s, the research on jointed rock mass has entered an era of rapid development. Reyes and Einstein (1991), Shen *et al*. (1995), Bobet and Einstein (1998a), Wong and Chau (1998), Yaylaci (2016, 2019); Yaylaci and Birinci (2013); Oner *et al*. (2015); Uzun Yaylacı *et al*. (2020), Lin (2020a-d), Hu *et al*. (2020); Cao *et al*. (2020); Lue *et al*. (2021); Zhang *et al*. (2020) and Shemirani *et al*. (2021) carried out a large number of two-dimensional crack compression and rock bridge fracture experiments with gypsum material to study the propagation mechanism of crack group under the influence of different factors such as geometric distribution, crack surface contact form, loading mode and path. Later, Prudencio and Jan (2007) carried out biaxial tests on physical models of rocks with non permanent joints. It is found that the failure mode

*Corresponding author, Ph.D., Associate Professor,
E-mail: vahab.sarfarazi@gmail.com

ISSN: 1738-1584 (Print), 1738-1991 (Online)

and the maximum strength depend on the geometry of the joints, the direction of the principal stress and the ratio of the intermediate stress to the compressive strength of the complete material. The test also shown that there are three basic failure modes: plane failure, step failure and new block rotation failure. Plane failure and stepped failure are related to high strength behavior and small failure strain, while rotational failure is related to very low strength, ductile behavior and large deformation. Wong and Einstein (2009) conducted a series of studies on crack initiation and rock bridge failure modes using gypsum and marble specimens, and summarized seven crack initiation modes and nine rock bridge connection modes. Yang *et al*. (2009) conducted uniaxial compression tests on pre-cracked marble samples with different configurations of preexisting flaws and identified eight types of coalescence patterns with tensile, shear, or mixed tensile–shear cracks. Zhou *et al*. (2014) experimental studied the failure modes of rock samples containing multiple flaws subjected to uniaxial compression and found five types of cracks and ten types of crack coalescence.

With the development of computer technology and numerical methods, a large number of numerical methods have been used to study the mechanical behavior of fractured rock mass. Bobet and Einstein (1998b) proposed a stress-based criterion for the initiation of tensile and shear cracks in elastic rock-like materials, and applied the criterion to FROCK (a hybrid indirect boundary element method) to simulate the initiation, propagation and coalescence of cracks. Tang and Kou (1998) modeled two particular cases concerning crack propagation and coalescence in brittle materials by using the rock failure process analysis code, RFPA(2D). Shen *et al*. (2004) developed the simulation software FRACOD based on displacement discontinuous boundary element (DDM), which has a good effect on the simulation of mode I and II crack propagation. Li and Wong (2012) analyzed the influences of pre-existing flaw inclination angle on the cracking processes based on finite element method (FEM) and non-linear dynamics method. Zhou *et al*. (2014) proposed a novel meshless numerical method, called general particle dynamics (GPD), and simulated the initiation, growth, and coalescence of cracks of rock-like brittle heterogeneous material containing four preexisting flaws under uniaxial compressive loads. Zhang *et al*. (2015) studied the fracture process of jointed rock slope based on fracture mechanics and strength reduction method (SRM), and analyzed the failure initiation of jointed rock slope by evaluating stress intensity factor (SIF). Considering fracture with different inclinations and hole with different positions, Wang and Tian (2018) modelled a variety of defective coal-rock specimens by PFC2D software, and analyzed the crack evolution law. Euser *et al*. (2019) utilized an in-house implementation of the combined finite-discrete element method (FDEM), known as the hybrid optimization software suite (HOSS), simulated the fracture coalescence processes of granite specimens with single or two flaws oriented at different angles.

The above researches play an important role in understanding the mechanical properties and failure behavior of jointed rock mass (single joint and combined joints). However, the joint characteristics of practical engineering are very complex, and there are still some joint characteristics that have not been considered in the existing research, such as triple-joint rock mass with different joint length and joint angle. In this paper, on the basis of the above research, firstly, the failure behavior and mechanical properties of triple joints with different fracture lengths and different fracture angles are studied by making rock like materials. Secondly, based on PFC2D, the failure and acoustic emission evolution characteristics of triple joint rock mass are analyzed. The results are helpful to further understand the instability mechanism of jointed rock mass.

2. Laboratory tests

2.1 Mechanical properties of rock-like materials

There are two disadvantages in using natural rock mass to study the failure behavior and mechanical properties of triple joints: one is that there are a large number of invisible cracks in natural rock mass, so it is difficult to ensure the homogeneity of triple-joint samples; the other is that it is difficult to make artificial joints in natural rock mass. In view of this, this paper uses rock like materials to simulate the failure behavior of triple joints. The rock like material is made of white cement and water according to the mass ratio of 2:1. Uniaxial compression test and Brazilian splitting

Table 1 Mechanical properties of rock-like materials

Elastic modulus, (GPa)	5
Poisson's ratio	0.18
UCS, (MPa)	7.4
Brazilian tensile strength (MPa)	1

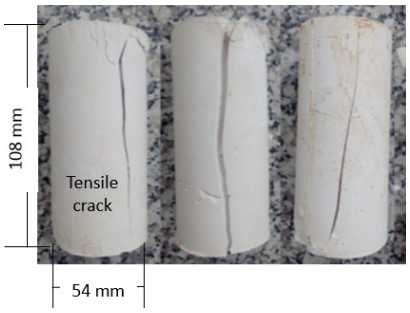

(a)

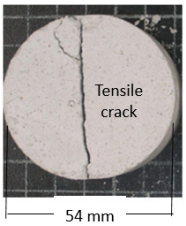

(b)

Fig. 1 Failure modes of rock-like material. (a) Uniaxial compression tests; (b) Brazilian splitting tests

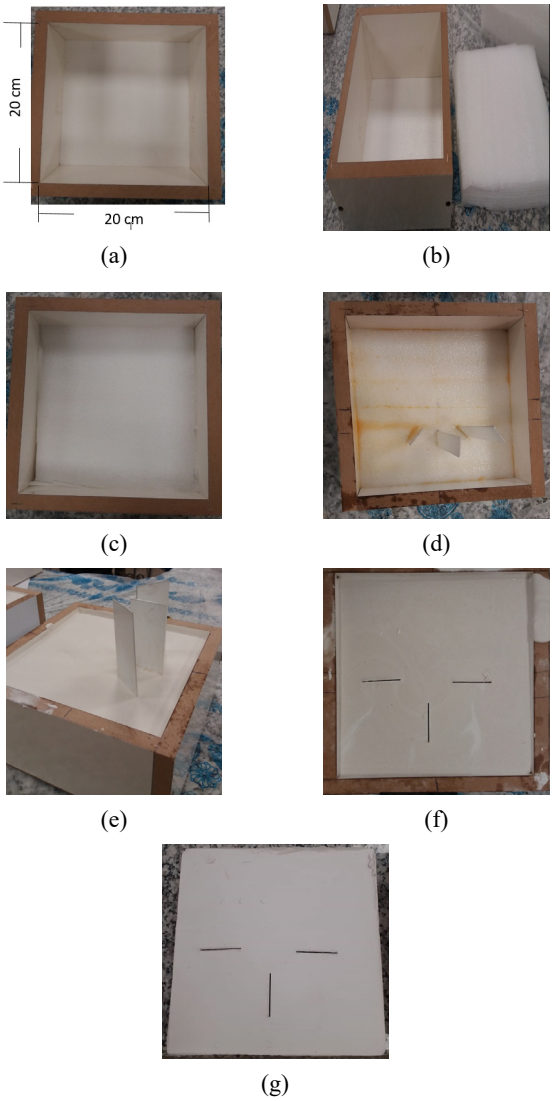

Fig. 2 (a) The frame with dimension of 20 cm × 20 cm × 10 cm; (b) and (c) a special plastic fiber with dimension of 20 cm × 20 cm × 50 cm was put into the frame; (d) the shim inside the plastic fiber; (e) slurry inside the box; (f) the aluminum sheet was removed from the mold, e) the physical specimen

test were carried out, and the mechanical properties of the material were obtained. The uniaxial compression specimen is a cylinder with a height of 10.8 cm and a diameter of 5.4 cm; the Brazilian splitting specimen is also a cylinder with a diameter of 54 mm and a thickness of 27 mm. Fig. 1 and Table 1 show the failure mode and mechanical properties of the artificial rock like material. Splitting failure occurs in this sample.

2.2 Triple joints samples

For triple samples, rock-like materials were used with the same material ratio in Section 2.1. The samples size (length × width × height) were both 20 cm × 20 cm × **5** cm. In the process of making the model, the configured pouring materials are poured into the mold at first; then, to create three open cracks, three thin metal plate is pre-

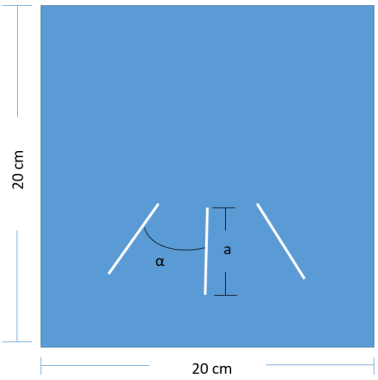

Fig. 3 Three echelon joints

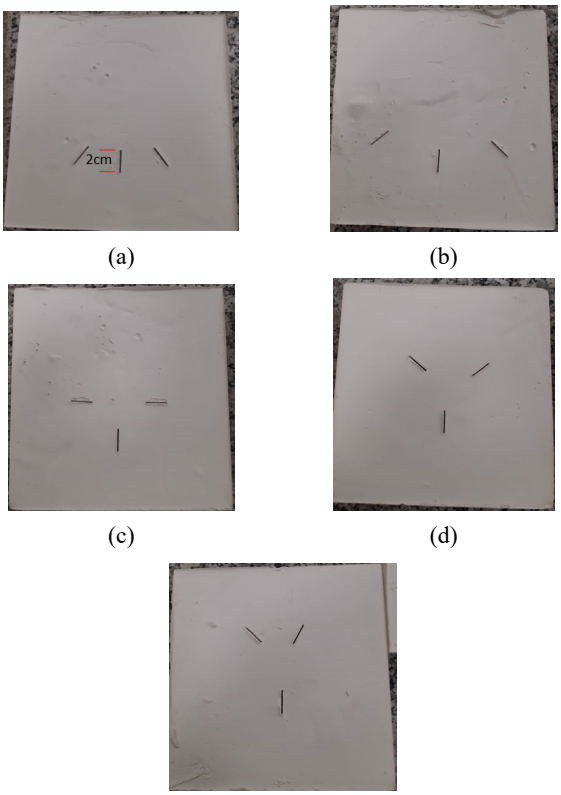

Fig. 4 Triple joints with angle of (a) 30°; (b) 60°; (c) 90°; (d) 120° and (e) 150°; joint length was 2 cm

inserting into the material and removing it after initial hardening of specimen (Fig. 2). Linear non-persistent cracks were formed in the model. The length of joint change from 2 cm to 6 cm with increments of 2 cm (a in Fig. 3). In constant joint length, the angle between the triple joints changes from 30° to 150° with increment of 30° (α in Fig. 3). The specimens were placed in a cool and ventilated condition for 28 days (Figs. 4-6).

2.3 Test equipment and loading

The electrohydraulic universal testing machine was used to performing the uniaxial compression test for the non-persistent joints. The experimental system includes the test

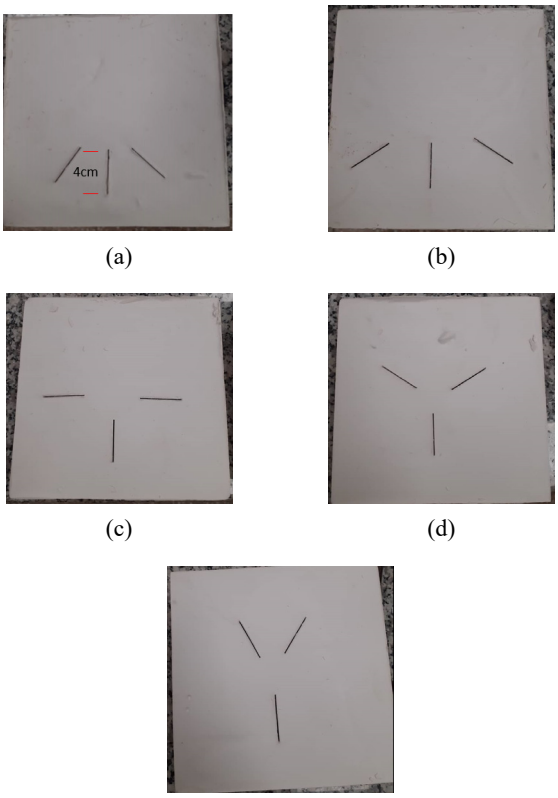

Fig. 5 Triple joints with angle of (a) 30°; (b) 60°; (c) 90°; (d) 120° and (e) 150°; joint length was 4 cm

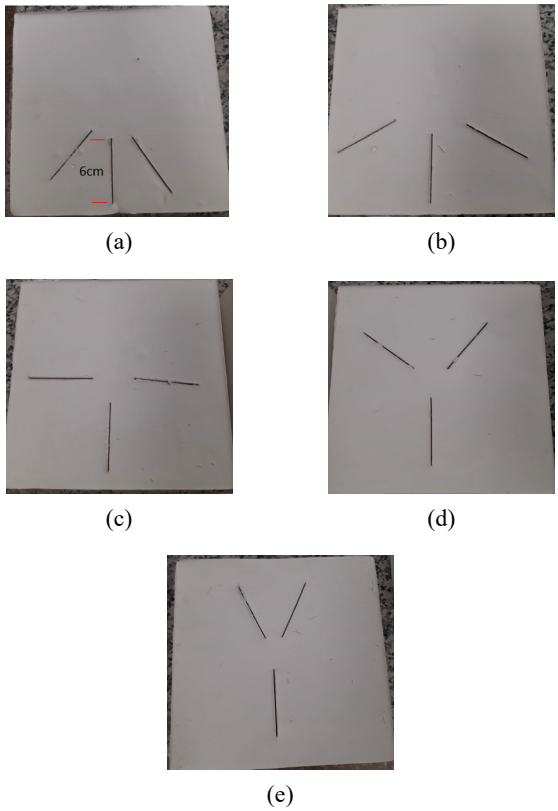

Fig. 6 Triple joints with angle of (a) 30°; (b) 60°; (c) 90°; (d) 120° and (e) 150°; joint length was 6 cm

Fig. 7 Specimen are placed between the plates of the loading machine

bed, loading control system and data acquisition system. The specimens were placed in the center of the base and maintained the horizontal contact with the base. During the experiment, the displacement loading rate was controlled to 0.05 mm/min (Fig. 7).

3. Experimental results

3.1 Failure pattern of experimental specimens

a) Joint length was 2 cm

Fig. 8 shows the failure pattern of specimens with oriented joint angle of 30°, 60°, 90°, 120° and 150°. When the angle between triple joint was 30 (Fig. 8(a)) and 60° (Fig. 8(b)), two wing shaped tensile cracks start from the directional joint and distribute parallel to the loading axis until they are combined with the boundary of the specimen. The vertical joint has little effect in failure process. When the angle between triple joint was 90° (Fig. 8(c)), four tensile wing cracks initiated from horizontal joint and propagated parallel to loading axis till integrated with boundaries of specimen. Also, one wing crack was initiated from vertical notch and propagated parallel to loading axis till integrated with boundaries of specimen. When the angle between triple joint was 120° (Fig. 8(d)) and 150° (Fig. 8(e)), two tensile wing cracks initiated from oriented joint and distributed parallel to loading axis till integrated with boundaries of sample. Also, one wing crack was initiated from vertical notch and propagated parallel to loading axis till integrated with boundaries of specimen. In these configurations, splitting failure was occurred in specimens. The failure surface was smooth without pulverized material. This is representative of tensile crack.

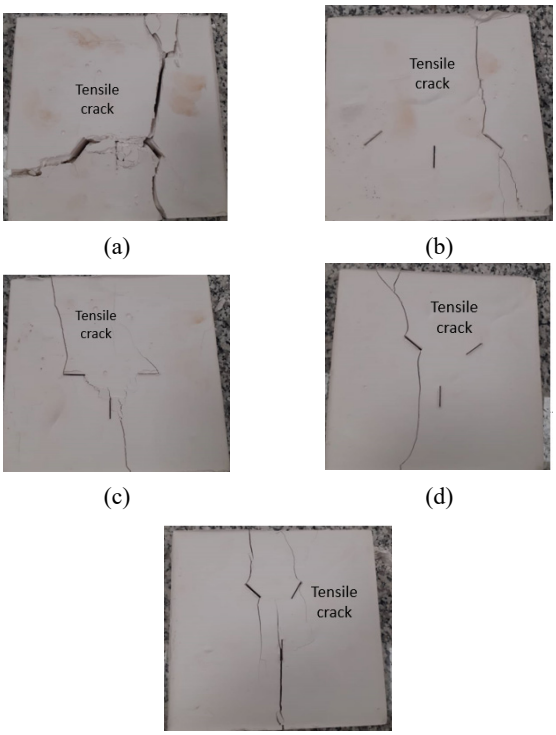

Fig. 8 Failure patterns of triple joints with angle of (a) 30°; (b) 60°; (c) 90°; (d) 120° and (e) 150°; joint length was 2 cm

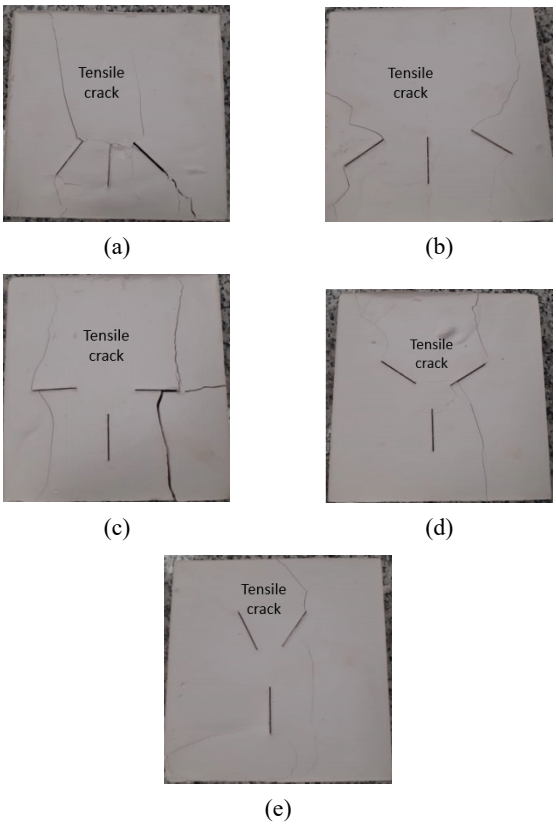

Fig. 9 Failure patterns of triple joints with angle of (a) 30°; (b) 60°; (c) 90°; (d) 120° and (e) 150°; joint length was 4 cm

b) Joint length was 4 cm

Fig. 9 shows the failure pattern of specimens with oriented joint angle of 30°, 60°, 90°, 120° and 150°. When the angle between triple joint was 30° (Fig. 9(a)) and 60° (Fig. 9(b)), two tensile wing cracks initiated from oriented joint and distributed parallel to loading axis till integrated with boundaries of specimen. The vertical joint has not any effect in failure process. When the angle between triple joint was 90° (Fig. 9(c)), four tensile wing cracks initiated from horizontal joint and propagated parallel to loading axis till integrated with boundaries of specimen. At the same time, a wing crack initiates from the vertical notch and propagates parallel to the loading axis until it is combined with the specimen boundary. When the angle between triple joint was 120° (Fig. 9(d)) and 150° (Fig. 9(e)), two wing shaped tensile cracks start from the directional joint and distribute parallel to the loading axis until they are combined with the boundary of the specimen. Also, one wing crack was initiated from vertical notch and propagated parallel to loading axis till integrated with boundaries of sample. In these configurations, splitting failure was occurred in sample. The Failure surface was smooth without pulverized material. This is representative of tensile crack.

c) Joint length was 6cm

Fig. 10 shows the failure pattern of specimens with oriented joint angle of 30°, 60°, 90°, 120° and 150°. When the angle between triple joint was 30° (Fig. 10(a)) and 60

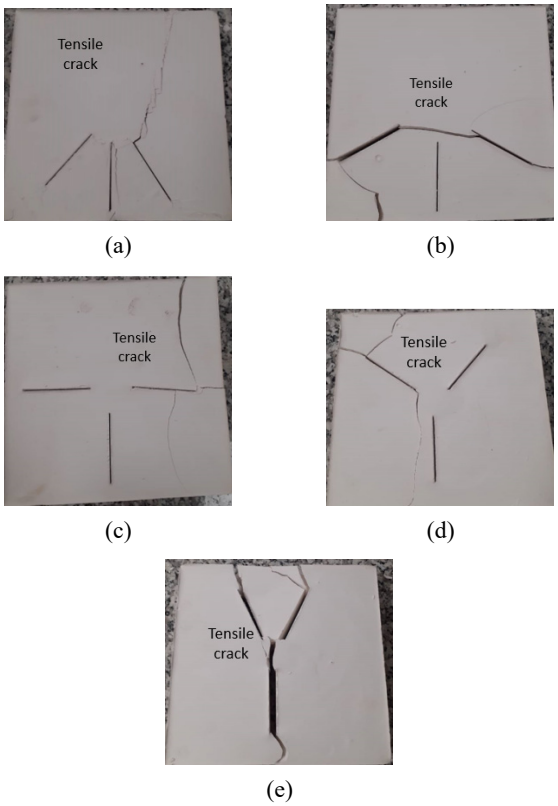

Fig. 10 Failure patterns of triple joints with angle of (a) 30°; (b) 60°; (c) 90°; (d) 120° and (e) 150°; joint length was 6 cm

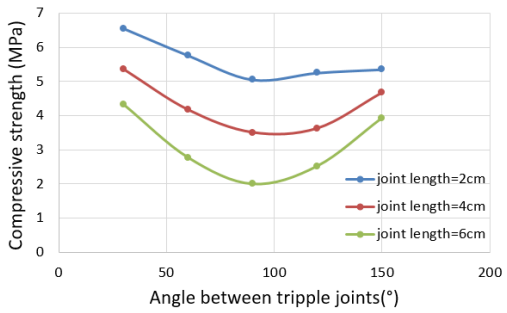

Fig. 11 Effect of angles and length of triple joints on UCS of different specimens

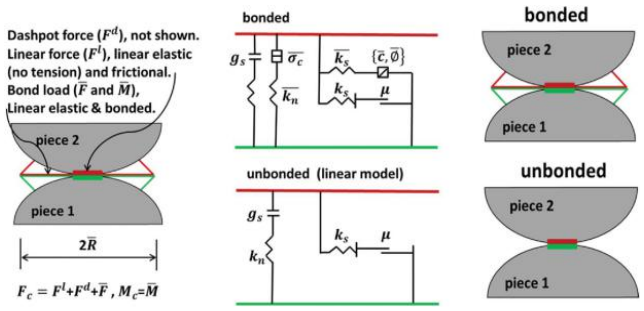

Fig. 12 Behavior of the grain-bonding system, Potyondy and Cundall 2004

(Fig. 10(b)), two wing shaped tensile cracks start from the directional joint and distribute parallel to the loading axis until they are combined with the boundary of the specimen. The vertical joint has little effect in failure process. When the angle between triple joint was 90° (Fig. 10(c)), four tensile wing cracks initiated from horizontal joint and propagated parallel to loading axis till integrated with boundaries of specimen. Also, one wing crack was initiated from vertical notch and propagated parallel to loading axis till integrated with boundaries of sample. When the angle between triple joint was 120° (Fig. 10(d)) and 150° (Fig. 10(e)), two tensile wing cracks initiated from oriented joint and distributed parallel to loading axis till integrated with boundaries of sample. Also, one wing crack was initiated from vertical notch and propagated parallel to loading axis till integrated with boundaries of sample. In these configurations, splitting failure was occurred in sample. The Failure surface was smooth without pulverized material. This is representative of tensile crack.

3.2 UCS of experimental specimens

Fig. 11 shows the effect of angles and length of triple-joint on the UCS of different specimens. This figure was presented for three joint length. The strength of samples was increased by decreasing the joint length. The minimum of compressive strength occurs when triple joint angle was 90°.

4. Numerical simulation

4.1 Particle flow code

In order to understand the failure mechanism of rock specimens with triple joints in more detail, this paper reproduced these models based on the particle flow code. PFC attempts to explain the mechanical properties and behaviors of media from a mesoscopic point of view, and has been widely used in rock engineering. In PFC2D, specimens are simulated by the collection of circular particles, and the mechanical properties of materials are simulated by the movement and interaction of particles (Potyondy and Cundall 2004). The radius of particles can be uniformly distributed or Gaussian distributed. There are two kinds of bonds that can be used to simulate the connection between rock particles, which are called contact bond (CB) and parallel bond (PB) (Wang and Tian 2018). In the contact bond model, particles are held together a point of glue and contacts cannot transfer torque. While in the parallel bond model particles are joined by surface layer of glue and contacts can tolerate torque that induced by particles rotation. Thus, the parallel bond model can represent a cement-like substance (Fig. 12), such as rock (Potyondy and Cundall 2004). The force between particles is reflected through the contact force chain and a bond breakage will occur then, when the local stresses exceed the parallel bond strength micro cracks are formed. In this paper, the PB model is used to simulate the triple-joint specimens.

4.2 Parameters for Rock-Like Material

Using PFC to carry out simulation experiment needs micro physical and mechanical parameters and bonding properties of particles. However, these parameters cannot be obtained directly from laboratory tests (Wang *et al*. 2016). Therefore, it is necessary to select and verify the micro parameters before numerical simulation. Usually, calibration of particles properties and parallel bonds in bonded particle model were carried out using Uniaxial compression and Brazilian tests (Ghazvinian *et al*. 2012) by "try and error" method. The model size should be similar as the experimental scale. For try and error processes, the value of porosity, expansion coefficient, friction coefficient and material pressure were fixed and then the tensile strength and compression strength of bonds were changed simultaneously. The model run with defined micro parameters. If the macro tensile strength and macro compressive strength get similar to experimental one, the model was calibrated. These micro parameters change till the numerical model be calibrated. Through a large number of numerical tests and comparative analysis with the experimental tests, it is found that the parameters in Table 2 can better reflect the mechanical properties of the test material.

Fig. 13 and Table 3 show the failure modes and mechanical properties of numerical intact rock-like material obtained by PFC2D simulation. Compared with Fig. 1 and Table 1, this parameter can better reflect the characteristics of test materials. These parameters will be used in the next numerical models.

Table 2 Micro properties used to represent the intact rock

Mechanical properties	Value	Mechanical properties	Value
Porosity	0.08	Elastic modulus (GPa)	0.17
Expansion coefficient	1.2	Friction coefficient	0.5
Density (kg/m^3)	2200	Tensile strength (MPa)	0.1
Minimum particle diameter (mm)	0.6	Tensile strength standard deviation (MPa)	0.01
Maximum particle diameter (mm)	1.2	Compressive strength (MPa)	0.5
Material pressure	0.1	Compressive strength standard deviation (MPa)	0.05

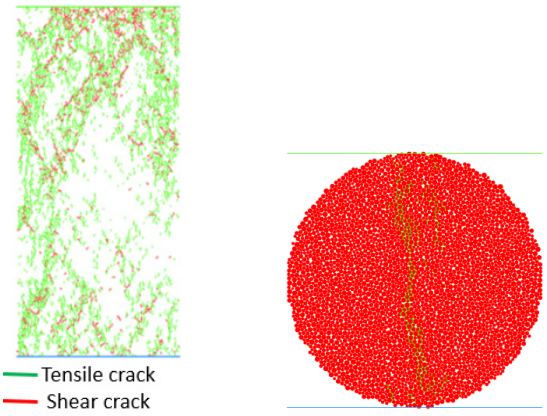

(a) (b)

Fig. 13 Failure modes of numerical intact rock-like material: (a) Uniaxial compression; (b) Brazilian tests

Table 3 Mechanical properties of PFC intact models

Elastic modulus, (GPa)	5
Poisson's ratio	0.19
UCS, (MPa)	7.4
Brazilian tensile strength (MPa)	1.05

4.3 Numerical models of triple joints

In order to further reveal the failure mechanism of three joint rock samples, this section reproduces the test model based on PFC2D, as shown in Figs. 14-16. The parameters of all numerical models are consistent with Table 2. All the PFC triple joints specimens had the dimensions of 20 cm × 20 cm. First, the model is filled with particles, then the non-persistent joints were formed by deletion of bands of particles from the model. The length of joint change from 2 cm to 6 cm with increments of 2 cm. In constant joint length, the angle between the tipple joints changes from 30° to 150° with increment of 30°. The small prefabricated crack in this experiment was 1 mm. Fifteen types of non-persistent joints were used in this numerical simulation.

After established the triple-joint model, upper and lower walls applied uniaxial force on the model. The axial load

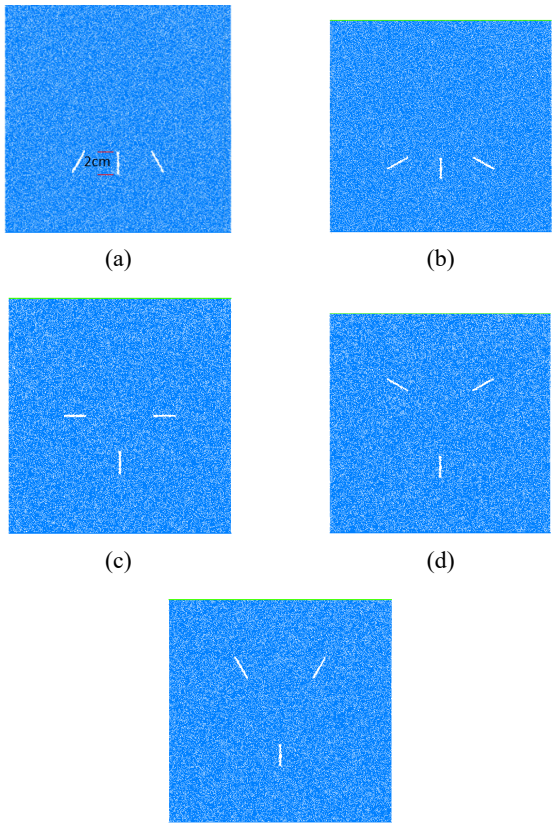

(a) (b) (c) (d) (e)

Fig. 14 Triple joints with angle of (a) 30°; (b) 60°; (c) 90°; (d) 120°; and (e) 150°; joint length was 2 cm

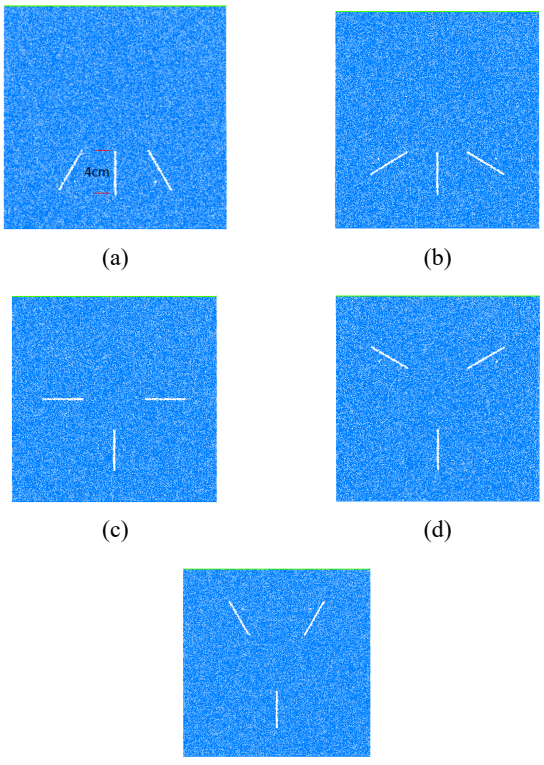

(a) (b) (c) (d) (e)

Fig. 15 Triple joints with angle of (a) 30°; (b) 60°; (c) 90°; (d) 120°; and (e) 150°; joint length was 4 cm

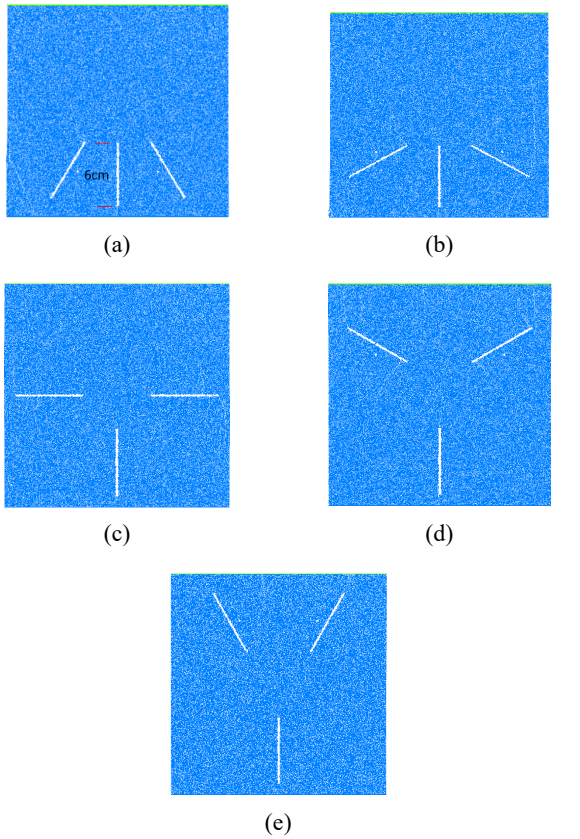

Fig. 16 Triple joints with angle of (a) 30°; (b) 60°; (c) 90°; (d) 120°; and (e) 150°; joint length was 6 cm

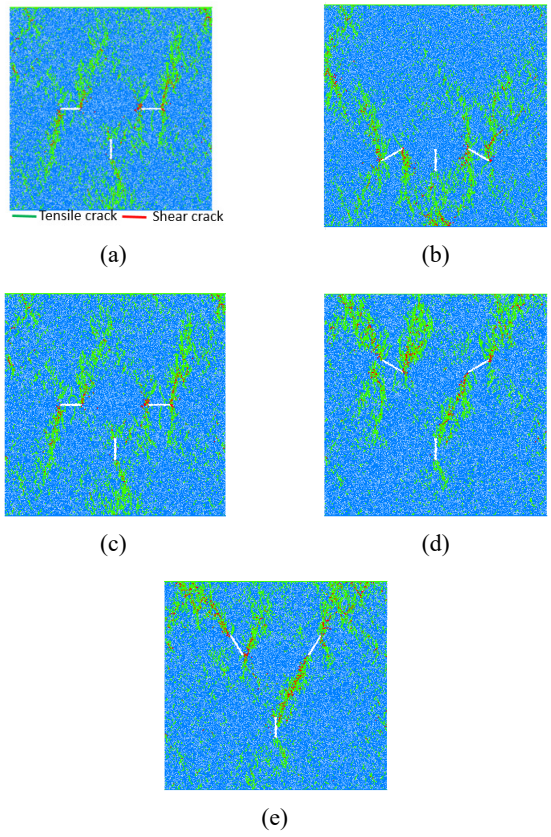

Fig. 17 Crack pattern in specimen containing triple joint with angle of (a) 30°; (b) 60°; (c) 90°; (d) 120°; and (e) 150°; joint length was 2 cm

rate on the model was 0.05 mm/min. The compression force was registered by taking the reaction forces on the upper wall.

4.4 Failure mechanism of numerical model

a) length of triple joint was 2 cm

Fig. 17 shows the failure pattern of specimens consisting triple joint with angle of 30°, 60°, 90°, 120° and 150° The green line and red line are representative of tensile crack and shear crack, respectively. Fig. 18 shows Ross diagram of crack growth. When the angles between triple joints was 30° (Fig. 17(a)) and 60° (Fig. 17(b)), four tensile cracks initiated from two oriented joints and propagated diagonally till integrated with sample boundary. In these configurations, the "v" shape columns of rock were separated from the model. When the angles between triple joints was 90° (Fig. 17(c)), four tensile cracks initiated from horizontal joints and propagated parallel to loading axis till integrated with sample boundary. In this configuration, the "I" shape columns of rock were separated from the model. When the angles between triple joints was 120 (Fig. 17(d)) and 150 (Fig. 17(e)), four tensile cracks initiated from two oriented joints and propagated diagonally till integrated with sample boundary. Also, one tensile crack initiated from vertical joint and propagated diagonally till coalescence with right oriented joints. In this configuration, both of the "I" shape and "v" shape columns of rock were separated from the model. From Fig. 17, the angles of micro cracks varied from 75 to 105 degree. The increasing the joint angle

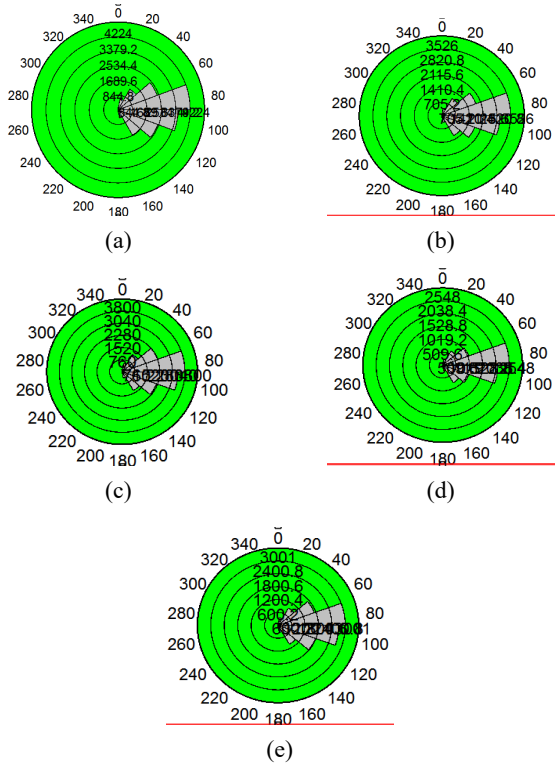

Fig. 18 Ross diagram of crack growth for triple joint with angle of (a) 30°; (b) 60°; (c) 90°; (d) 120°; and (e) 150°

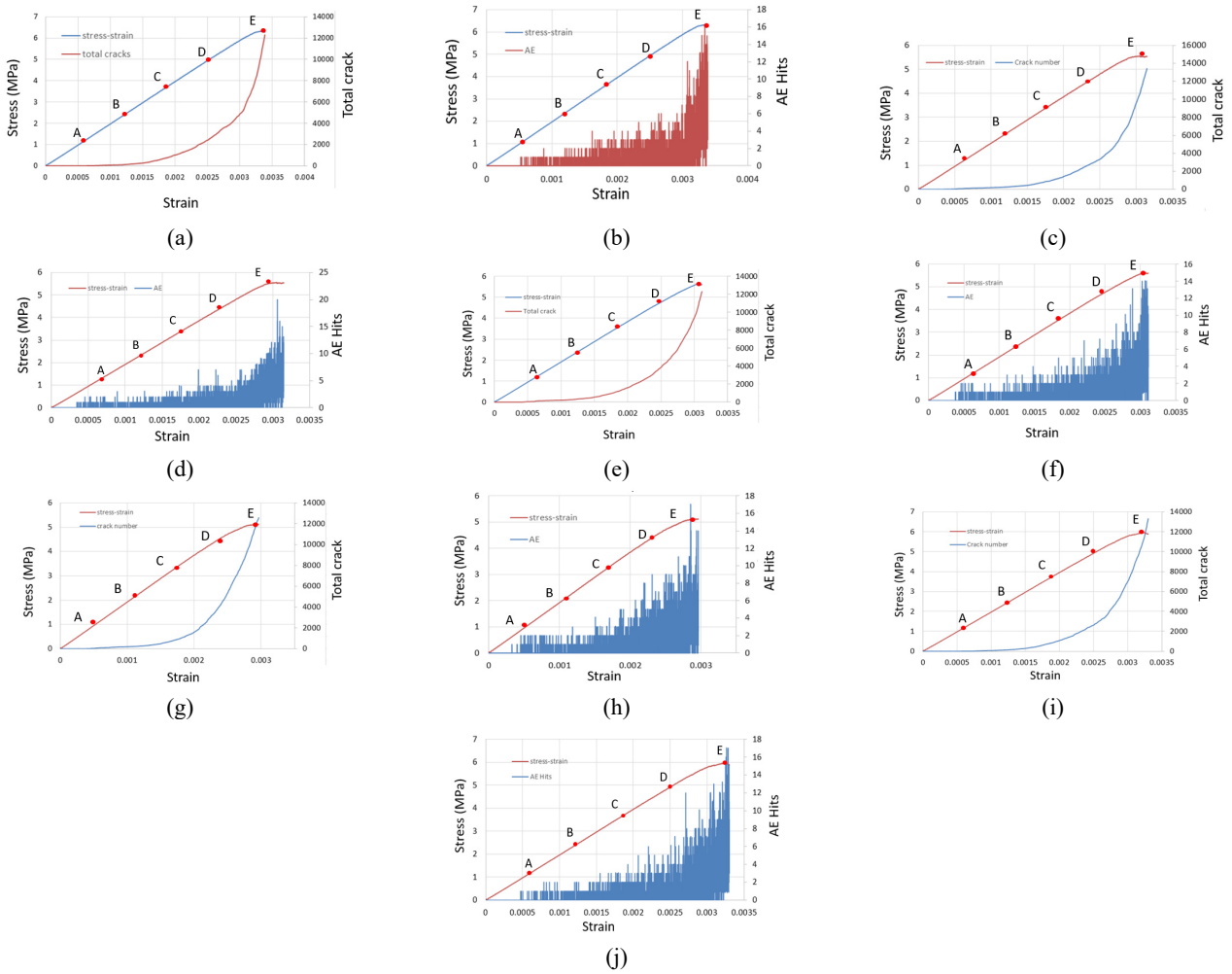

Fig. 19 Stress and AE behavior in the test simulation for joint length of 2 cm: (a), (c), (e), (g), (i) stress-strain curve and cumulative crack number for joint angle of 30°, 60°, 90°, 120° and 150°; (b), (d), (f), (h), (j) the number of AE hits along the strain curve for joint angle of 30°, 60°, 90°, 120° and 150°

have little effect on the newborn crack numbers, similar as the experimental tests.

Figs. 19(a), (c), (e), (g) and (i) show the stress-strain curve along with the total crack number for joint angles of 30°, 60°, 90°, 120° and 150°. Figs. 19(b), (d), (f), (h) and (j) show the stress-strain curve along with AE hits for joint angles of 30°, 60°, 90°, 120° and 150°. The reason why we analyze the acoustic emission characteristics (AE hits) of jointed rock mass in the process of compression is that the engineering rockburst problem is often monitored based on the AE signal in practical engineering. This value was chosen to cover all of the stress path. In other word in elastic, yield, plastic and final failure stages, the stress increment and AE were analyzed. In the PFC model, when the stress between particles is greater than the PB model contact strength, the fracture occurs, that is, an AE hit occurs (Zhang *et al*. 2018). Therefore, the acoustic emission phenomenon can be simulated by writing fish language to monitor the fracture of the model. Along the stress-strain curve, five points labeled A-E were marked, and the stress at each point are 20%, 40%, 60%, 80% and 100% of total stress, respectively. The corresponding points were also marked in Figs. 19(b), (d), (f), (h) and (j). It can be seen from the figure that with the increase of stress-strain curve until the peak, the AE hits of triple joints numerical specimens presents three stages. In the first stage, stress less than point A, AE hits is almost zero; this stage is in the elastic stage, and there is no crack in the specimen. In the second stage, the stress is about between point A and point C. In this stage, AE hits is in a slowly increasing stage, which is due to the micro cracks in the jointed rock mass continuous expansion.

In the third stage, after the C point, the AE hits increase rapidly, because the rock almost enters its bearing limit and the crack propagation speed is very fast. Generally, the maximum value of AE is near the peak value. When the joint length is the same, different joint angle does not lead to a significant change in the maximum AE hits. It shows that the joint angle changes the failure mode of jointed rock sample, but has little effect on the evolution of AE. In constant joint length, the strain value in maximum stress stage was constant by increasing the joint angle.

b) Length of triple joint was 4cm

Fig. 20 shows the failure pattern of specimens consisting triple joint with angle of 30°, 60°, 90°, 120° and

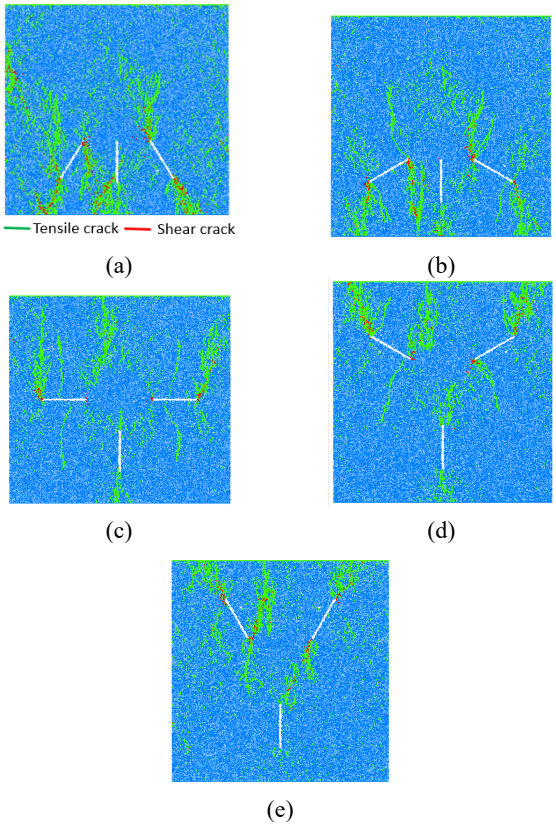

Fig. 20 Crack pattern in specimen containing triple joint with angle of (a) 30°; (b) 60°; (c) 90°; (d) 120° and (e) 150°; joint lengths were 4 cm

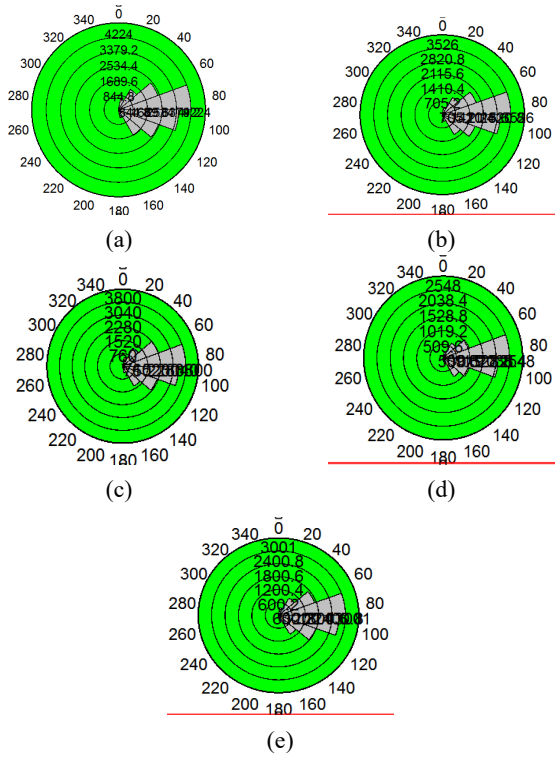

Fig. 21 Ross diagram of crack growth for triple joint with angle of (a) 30°; (b) 60°; (c) 90°; (d) 120° and (e) 150°

150°. The green line and red line are representative of tensile crack and shear crack, respectively. Fig. 21 shows Ross diagram of crack growth. When the angles between triple joints was 30° (Fig. 20(a)) and 60° (Fig. 20(b)), four tensile cracks initiated from two oriented joints and propagated diagonally till integrated with sample boundary. Also, one tensile crack initiated from vertical joint and propagated vertically till coalescence with lower model boundary. In these configurations, the "v" shape columns of rock were separated from the model. When the angles between triple joints was 90° (Fig. 20(c)), four tensile cracks initiated from horizontal joints and propagated parallel to loading axis till integrated with sample boundary. In this configuration, the "I" shape columns of rock were separated from the model. When the angles between triple joints was 120° (Fig. 20(d)) and 150° (Fig. 20(e)), four tensile cracks initiated from two oriented joints and propagated diagonally till integrated with sample boundary. Also, one tensile crack initiated from vertical joint and propagated diagonally till coalescence with right oriented joints. In this configuration, both of the "I" shape and "v" shape columns of rock were separated from the model. From Fig. 21, the angles of micro cracks varied from 75 to 105 degree. The increasing of joint angle has not any effect on the newborn crack numbers.

Figs. 22(a), (c), (e), (g) and (i) show the stress-strain curve along with the total crack number, and Figs. 22(b), (d), (f), (h) and (j) show the stress-strain curve along with AE hits. Along the stress-strain curve, five points labeled A-E were marked, and the stress at each point are 20%, 40%, 60%, 80% and 100% of total stress, respectively. The corresponding points were also marked in Figs. 22(b), (d), (f), (h) and (j).

In general, when the joint length is 4 cm, the crack accumulation and AE hits evolution process of jointed rock mass also show a gradually increasing trend. However, the evolution characteristics of AE hits are slightly different from that of specimens with 2 cm joint length. When the joint angle is 30° and 150°, the evolution process of AE hits is similar to that of 2 cm specimen. There are three stages, including zero AE hits stage, slow increase stage and rapid increase stage. However, when the joint angle is 60°, 90° and 120°, the second stage of AE hits does not increase slowly, but there are multiple peaks, which is caused by the continuous step expansion of the cracks. This shows that the crack propagation is greatly affected by the increase of joint length. In addition, in general, the change of joint angle does not lead to the sudden jump of the maximum AE hits. This important is similar to the result of joint length of 2 cm. In constant joint length, the strain value in maximum stress stage was constant by increasing the joint angle. The newborn crack numbers were decreased by increasing the joint length.

c) Length of triple joint was 6cm

Fig. 23 shows the failure pattern of specimens consisting triple joint with angle of 30°, 60°, 90°, 120° and 150°. The green line and red line are representative of tensile crack and shear crack, respectively. Fig. 24 shows Ross diagram of crack growth. When the angles between

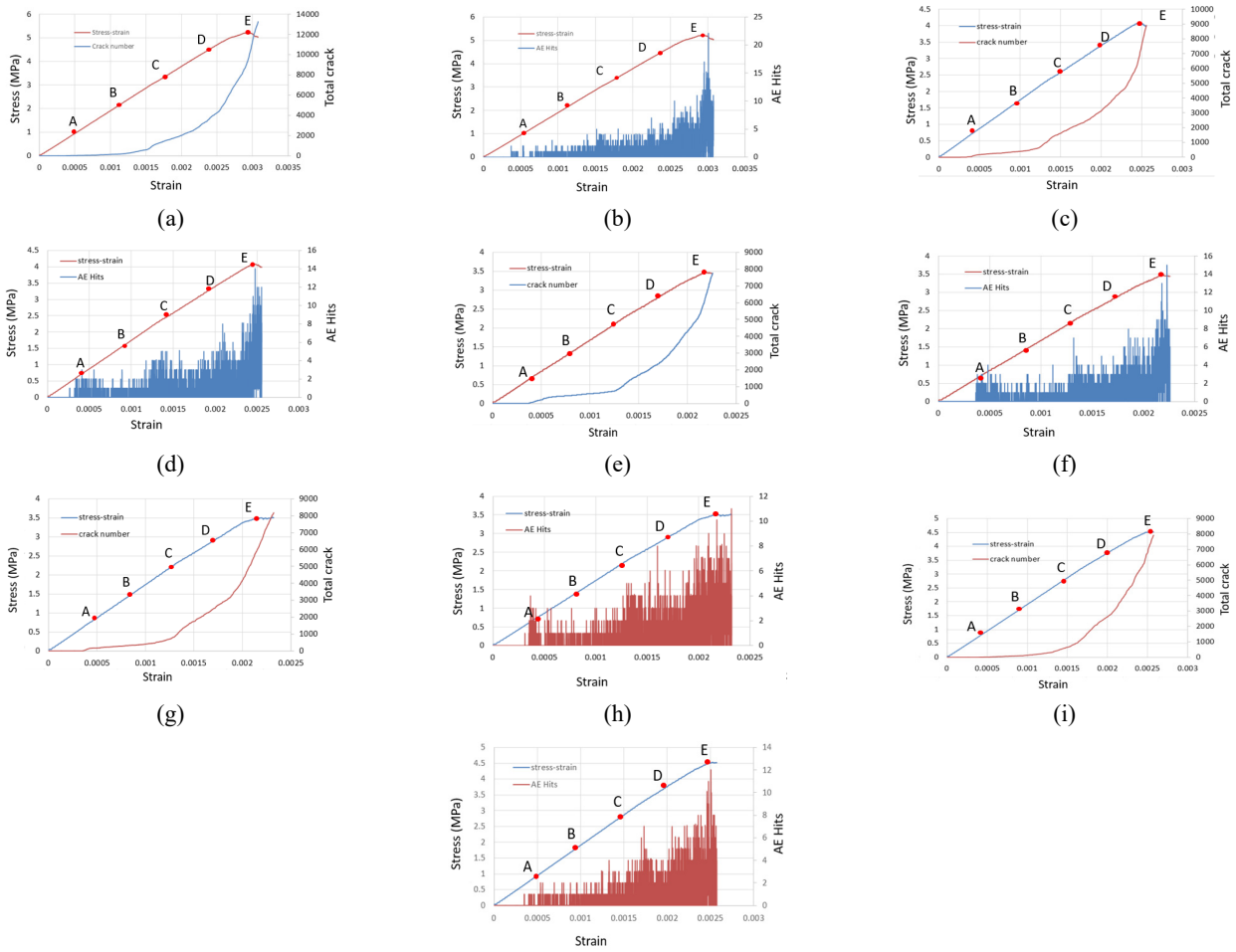

Fig. 22 Stress and AE behavior in the test simulation for joint length of 4 cm: (a), (c), (e), (g), (i) stress-strain curve and cumulative crack number for joint angle of 30°, 60°, 90°, 120° and 150°; (b), (d), (f), (h), (j) the number of AE hits along the strain curve for joint angle of 30°, 60°, 90°, 120° and 150°

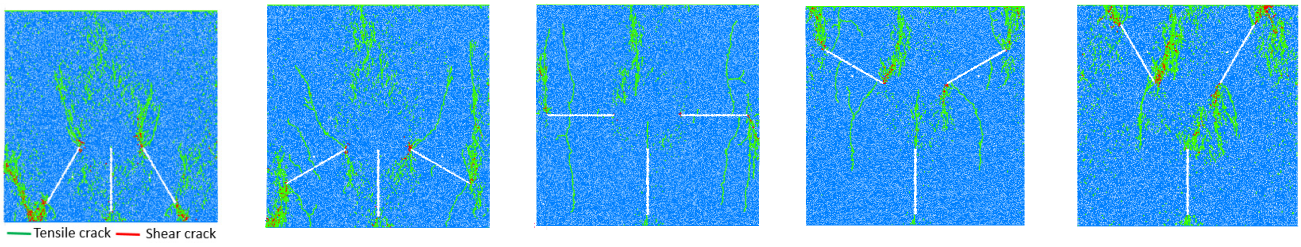

Fig. 23 Crack pattern in specimen containing triple joint with angle of (a) 30°; (b) 60°; (c) 90°; (d) 120° and (e) 150°; joint lengths were 6 cm

triple joints was 30° (Fig. 23(a)) and 60° (Fig. 23(b)), four tensile cracks initiated from two oriented joints and propagated diagonally till integrated with sample boundary.

Also, one tensile crack initiated from vertical joint and propagated vertically till coalescence with lower model boundary. In these configurations, the "v" shape columns of rock were separated from the model. When the angles between triple joints was 90° (Fig. 23(c)), four tensile cracks initiated from horizontal joints and propagated parallel to loading axis till integrated with sample boundary. In this configuration, the "I" shape columns of rock were separated from the model. When the angles between triple joints was 120° (Fig. 23(d)) and 150° (Fig. 23(e)), four tensile cracks initiated from two oriented joints and propagated diagonally till integrated with sample boundary. Also, one tensile crack initiated from vertical joint and propagated diagonally till coalescence with right oriented joints. In this configuration, both of the "I" shape and "v" shape columns of rock were separated from the model. From Fig. 24, the angles of micro cracks varied from 75 to

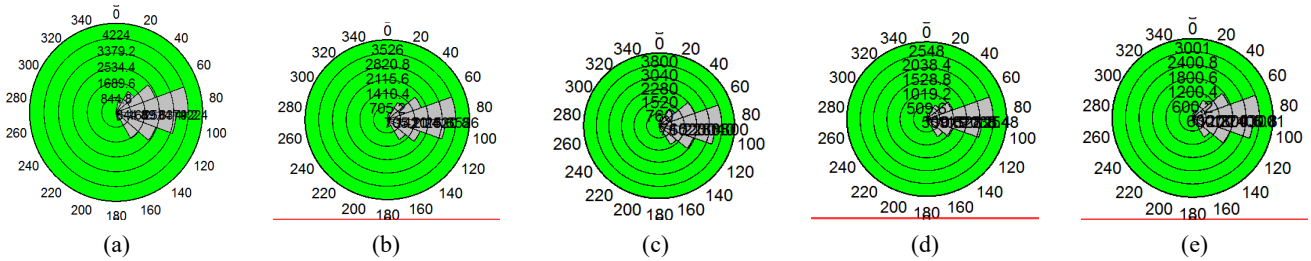

(a) (b) (c) (d) (e)

Fig. 24 Ross diagram of crack growth for triple joint with angle of (a) 30°; (b) 60°; (c) 90°; (d) 120° and (e) 150°

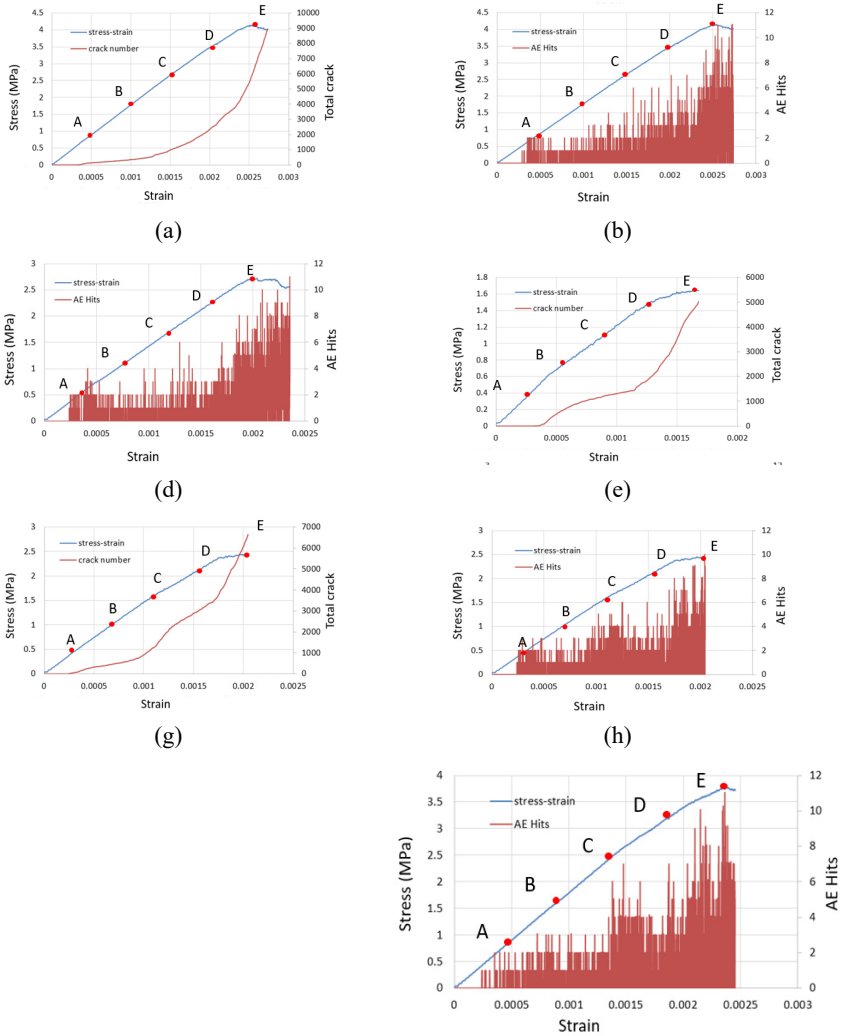

(a) (b) (c) (d) (e) (f) (g) (h) (i) (j)

Fig. 25 Stress and AE behavior in the test simulation for joint length of 6 cm: (a), (c), (e), (g), (i) stress-strain curve and cumulative crack number for joint angle of 30°, 60°, 90°, 120° and 150°; (b), (d), (f), (h), (j) the number of AE hits along the strain curve for joint angle of 30°, 60°, 90°, 120° and 150°

105 degree. The increasing of joint angle has not any effect on the newborn crack numbers.

By comparison between Figs. 8-10 and Figs. 17, 20 and 23, It can be concluded that failure pattern is similar in both of the experimental test and numerical simulation.

Figs. 25(a), (c), (e), (g) and (i) show the stress-strain curve along with the total crack number, and Figs. 25(b), (d), (f), (h) and (j) show the stress-strain curve along with AE hits. Along the stress-strain curve, five points labeled A-E were marked, and the stress at each point are 20%, 40%, 60%, 80% and 100% of total stress, respectively. The corresponding points were also marked in Figs. 25(b), (d), (f), (h) and (j). The same results were occurred in these configurations.

4.2 UCS of numerical specimens

Fig. 26 shows the effect of triple joint angle on the

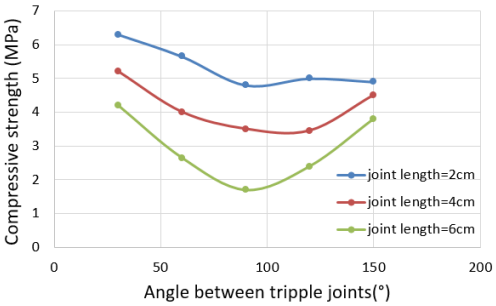

Fig. 26 The effect of joint angle on the strength of models

strength of numerical models. This figure was presented for three joint lengths. The strength of samples was increased by decreasing the joint length. The minimum of compressive strength occurs when triple joint angle was 90°.

By comparison between Figs. 11 and 26. It can be concluded that failure strength is nearly similar in both of the experimental test and numerical simulation.

5. Conclusions

In this paper, the failure mode, mechanical properties and AE characteristics of rock specimens with triple joints are analyzed based on experiments and PFC2D. The main conclusions are as follow.

(1) When the angles between triple joints was 30° and 60°, four tensile cracks initiated from two oriented joints and propagated diagonally till integrated with sample boundary. In these configurations, the "v" shape columns of rock were separated from the model. When the angles between triple joints was 90°, four tensile cracks initiated from horizontal joints and propagated parallel to loading axis till integrated with sample boundary. In this configuration, the "I" shape columns of rock were separated from the model. When the angles between triple joints was 120° and 150°, four tensile cracks initiated from two oriented joints and propagated diagonally till integrated with sample boundary. Also, one tensile crack initiated from vertical joint and propagated diagonally till coalescence with right oriented joints. In this configuration, both of the "I" shape and "v" shape columns of rock were separated from the model.

(2) The angles of micro cracks varied between 75 and 105 degree. The newborn crack numbers were decreased by increasing the joint length. The newborn crack numbers were nearly constant by increasing the joint angle. The branching of new born cracks was decreased by increasing the joint length. In a large notch length condition, the notch tip will be close to model boundary so one major fracture leads to final failure. In other cases, too many cracks were initiated in the model due to presence of large intact area between the notch and model boundary.

(3) In constant joint length, the strain value in maximum stress stage was constant by increasing the joint angle. Also, the strain value in maximum stress stage was decreased by increasing the joint length. The minimum of compressive strength occurs when triple joint angle was 90°. The strength of sample was decreased by increasing the joint length.

(4) With the increase of stress, the cumulative crack curve and AE hits evolution curve of tested specimens increase. Especially, when the joint length is 2 cm, the increase of these curves is relatively smooth and the fluctuation is small. However, with the increase of crack length, the fluctuation of crack accumulation curve and AE evolution curve increases gradually. The larger the crack length is, the smaller the maximum AE hits is. This shows that the larger the joint, the lower the energy required for crack propagation and failure. When the crack angle is 60°, 90° and 120°, the fluctuation of cumulative crack curve and AE hits curve will be aggravated, but the maximum number of AE hits will not increase.

(5) The crack propagation is greatly affected by the increase of joint length. In addition, in general, the change of joint angle does not lead to the sudden jump of the maximum AE hits.

References

Ashby, M.F. and Hallam, S.D. (1986), "The failure of brittle solids containing small cracks under compressive stress states", *Acta Metallurgica*, **34**(3), 497-510. https://doi.org/10.1016/0001-6160(86)90086-6

Bobet, A. and Einstein, H.H. (1998a), "Failure coalescence in rock-type material under uniaxial and biaxial compression", *Int. J. Rock Mech. Min. Sci.*, **35**(7), 863-888. https://doi.org/10.1016/S0148-9062(98)00005-9

Bobet, A. and Einstein, H.H. (1998b), "Numerical modeling of fracture coalescence in a model rock material", *Int. J. Fract.*, **92**, 221-252. https://doi.org/10.1023/A:1007460316400

Brace, W.F. and Bombolakis, E.G. (1963), "A note on brittle crack growth in compression", *J. Geophys. Res.*, **68**(12), 3709- 3713. https://doi.org/10.1029/JZ068i012p03709

Cao, R., Yao, R., Meng, J., Lin, Q., Lin, H. and Li, S. (2020), "Failure mechanism of non-persistent jointed rock like specimens under uniaxial loading: laboratory testing", *Int. J. Rock Mech. Min. Sci.*, **132**, 104314. https://doi.org/10.1016/j.ijrmms.2020.104341

Euser, B., Rougier, E., Lei, Z., Knight, E.E., Frash, L.P., Carey, J.W., Viswanathan, H. and Munjiza, A. (2019), "Simulation of fracture coalescence in granite via the combined finite–discrete element method", *Rock Mech. Rock Eng.*, **52**(9), 3213-3227. https://doi.org/10.1007/s00603-019-01773-0

Ghazvinian, A., Sarfarazi, V., Schubert, W. and Blumel, M. (2012), "A study of the failure mechanism of planar non-persistent open joints using PFC2D", *Rock Mech. Rock Eng.*, **45**(5), 677-693. https://doi.org/10.1007/s00603-012-0233-2

Hu, J., Wen, G., Lin, Q., Cao, P. and Li, S. (2020), "Mechanical properties and crack evolution of double-layer composite rock-like specimens with two parallel fissures under uniaxial compression", *Theor. Appl. Fract. Mech.*, **108**, 102610. https://doi.org/10.1016/j.tafmec.2020.102610

Lajtai, E.Z. (1971), "A theoretical and experimental evaluation of the Griffith theory of brittle fracture", *Tectonophysics*, **11**(2), 129-156. https://doi.org/10.1016/0040-1951(71)90060-6

Li, H. and Wong, L.N.Y. (2012), "Influence of flaw inclination angle and loading condition on crack initiation and propagation", *Int. J. Solids Struct.,* **49**(18), 2482-2499. https://doi.org/10.1016/j.ijsolstr.2012.05.012

Lin, Q. (2020a), "Mechanical behavior around double circular openings in a jointed rock mass under uniaxial compression", *Arch. Civil Mech. Eng.,* **20**, 19-32. https://doi.org/10.1007/s43452-020-00027-z

Lin, Q. (2020b), "Crack coalescence in rock-like specimens with two dissimilar layers and pre-existing double parallel joints under uniaxial compression", *Int. J. Rock Mech. Min. Sci*., **139**, 104621. https://doi.org/10.1016/j.ijrmms.2021.104621

Lin, Q. (2020c), "Fatigue behaviour and constitutive model of yellow sandstone containing pre-existing surface crack under uniaxial cyclic loading", *Theor. Appl. Fract. Mech*., **109**, 102776. https://doi.org/10.1016/j.tafmec.2020.102776

Lin, Q. (2020d), "Strength and failure characteristics of jointed rock mass with double circular holes under uniaxial compression: Insights from discrete element method modelling", *Theor. Appl. Fract. Mech.,* **109**(7), 102692. https://doi.org/10.1016/j.tafmec.2020.102692

Lue, X., Cao, P. and Lin, Q. (2021), "Mechanical behaviour of fracture-filled rock-like specimens under compression-shear loads: An experimental and numerical study", *Theor. Appl. Fract. Mech*., **113**, 102935. https://doi.org/10.1016/j.tafmec.2021.102935

Oner, E., Yaylaci, M. and Birinci, A. (2015), "Analytical solution of a contact problem and comparison with the results from FEM", *Struct. Eng. Mech., Int. J*., **54**(4), 607-622. https://doi.org/10.12989/sem.2015.54.4.000

Potyondy, D.O. and Cundall, P.A. (2004), "A bonded-particle model for rock", *Int. J. Rock Mech. Min. Sci*., **41**, 1329-1364. https://doi.org/10.1016/j.ijrmms.2004.09.011

Price, N.J. (1966), *Fault and joint development in brittle and semi-brittle rock*, London: Permagon Press Ltd.

Prudencio, M. and Jan, M.V.S. (2007), "Strength and failure modes of rock mass models with non-persistent joints", *Int. J. Rock Mech. Min. Sci.,* **44**(6), 890-902. https://doi.org/10.1016/j.ijrmms.2007.01.005

Reyes, O. and Einstein, H.H. (1991), "Failure mechanism of fractured rock-a fracture coalescence model", *Proceedings of 7th International Congress of Rock Mechanics*, pp. 333-340.

Shemirani, A.B., Amini, M.S., Sarfarazi, V., Shahriar, K., Moarefvand, P. and Haeri, H. (2021), "Experimental and numerical investigation of the effect of bridge area and its angularities on the failure mechanism of non-persistent crack in concrete-like materials", *Smart Struct. Syst*., *Int. J.,* **27**(3), 54-67. https://doi.org/10.12989/sss.2021.27.3.479

Shen, B., Stephansson, O., Einstein, H.H. and Ghahreman, B. (1995), "Coalescence of fractures under shear stresses in experiments", *J. Geophys. Res*., **100**(6), 5975-5990. https://doi.org/10.1029/95JB00040

Shen, B., Stephansson, O., Rinne, M., Lee, H.S., Jing, L. and Roshoff, K. (2004), "A fracture propagation code and its applications to nuclear waste disposal", *Int. J. Rock Mech. Min. Sci.,* **41**(3), 448-449. https://doi.org/10.1016/j.ijrmms.2004.03.085

Tang, C.A. and Kou, S.Q. (1998), "Crack propagation and coalescence in brittle materials under compression", *Eng. Fract. Mech*., **61**(3-4), 311-324. https://doi.org/10.1016/S0013-7944(98)00067-8

Wang, X. and Tian, L.G. (2018), "Mechanical and crack evolution characteristics of coal–rock under different fracture-hole conditions: a numerical study based on particle flow code", *Environ. Earth Sci*., **77**(8), 1-10. https://doi.org/10.1007/s12665-018-7486-3

Wang, X., Wen, Z.J. and Jiang, Y.J. (2016), "Time–space effect of stress field and damage evolution law of compressed coal-rock", *Geotech. Geol. Eng*., **34**(6), 1933-1940. https://doi.org/10.1007/s10706-016-0074-y

Wong, R.H. and Chau, K.T. (1998), "Crack coalescence in a rock-like material containing two cracks", *Int. J. Rock Mech. Min. Sci*., **35**(2), 147-164. https://doi.org/10.1016/S0148-9062(97)00303-3

Wong, L.N.Y. and Einstein, H.H. (2009), "Crack coalescence in molded gypsum and Carrara marble: part 1. Macroscopic observations and interpretation", *Rock Mech. Rock Eng*., **42**(3), 475-511. https://doi.org/10.1007/s00603-008-0002-4

Yang, S.Q., Dai, Y.H., Han, L.J. and Jin, Z.Q. (2009), "Experimental study on mechanical behavior of brittle marble samples containing different flaws under uniaxial compression", *Eng. Fract. Mech.,* **76**(12), 1833-1845. https://doi.org/10.1016/j.engfracmech.2009.04.005

Yaylaci, M. (2016), "The investigation crack problem through numerical analysis", *Struct. Eng. Mech., Int. J*., **57**(6), 1143-1156. https://doi.org/10.12989/sem.2016.57.6.1143

Yaylacı, M. (2019), "Numerical analysis of the receding contact problem of two bonded layers resting on an elastic half plane", *Struct. Eng. Mech., Int. J*., **72**(6), 111-123. https://doi.org/10.12989/sem.2019.72.6.775

Yaylaci, M. and Birinci, A. (2013), "The receding contact problem of two elastic layers supported by two elastic quarter planes", *Struct. Eng. Mech., Int. J*., **48**(2), 241-255. https://doi.org/10.12989/sem.2013.48.2.241

Yaylacı, E.U., Yaylacı, M., Ölmez, H. and Birinci, A. (2020), "Artificial neural network calculations for a receding contact problem", *Comput. Concrete, Int. J.,* **25**(6), 77-89. https://doi.org/10.12989/cac.2020.25.6.077

Zhang, K., Cao, P., Meng, J., Li, K. and Fan, W. (2015), "Modeling the progressive failure of jointed rock slope using fracture mechanics and the strength reduction method", *Rock Mech. Rock Eng.,* **48**(2), 771-785. https://doi.org/10.1007/s00603-014-0605-x

Zhang, Q., Wang, X., Tian, L.G. and Huang, D.M. (2018), "Analysis of mechanical and acoustic emission characteristics of rock materials with double-hole defects based on particle flow code", *Shock Vib.,* **32**(1), 23-35. https://doi.org/10.1155/2018/7065029

Zhang, X., Bayat, V., Koopialipoor, M., Armaghani, D.J., Yong, W. and Zhou, J. (2020), "Evaluation of structural safety reduction due to water penetration into a major structural crack in a large concrete project", *Smart Struct. Syst., Int. J.,* **26**(3), 90-108. https://doi.org/10.12989/sss.2020.26.3.319

Zhou, X.P., Cheng, H. and Feng, Y.F. (2014), "An experimental study of crack coalescence behaviour in rock-like materials containing multiple flaws under uniaxial compression", *Rock Mech. Rock Eng.,* **47**(6), 1961-1986. https://doi.org/10.1007/s00603-013-0511-7

Zhou, X.P., Bi, J. and Qian, Q.H. (2015), "Numerical simulation of crack growth and coalescence in rock-like materials containing multiple pre-existing flaws", *Rock Mech. Rock Eng.,* **48**(3), 1097-1114. https://doi.org/10.1007/s00603-014-0627-4

CC